Second Harmonic Generation in Solid-State Materials

Galan Moody

Alan D. Bristow, Steven T. Cundiff

Summer 2007

Abstract

Solid-state materials are examined as a function of azimuthal angle using optical second harmonic generation (SHG). Understanding crystal symmetries and surface boundary conditions is pertinent in order to identify the relationship between $\chi^{(2)}$ tensor elements and bulk and surface contributions. SHG from GaAs (111) and Si (100) was examined as a function of azimuthal angle and circular dichroism was observed in both. This work provides thorough experimental characterization of the setup which is intended for future SHG studies on more complex electronic systems.

1. Introduction

A primary goal for studying solid-state materials is to gain a better understanding of the fundamental properties of matter. More specifically, understanding crystal symmetries and boundary conditions at surfaces is crucial for understanding the relationship between bulk and surface contributions to the second order electric susceptibility tensor elements $(\chi^{(2)})$[1]. Additionally, studying how these different tensor elements interfere due to phase-mismatching of their excitations helps elucidate properties of the material.

Gallium arsenide (111) is an appropriate material to study crystal symmetries because 481.44 T44.0(r)-17.0(y)-316.0(c)4.0(ont)-1.9(r)3.0(i)-1.9(but)-oo0(i)der to

symmetries and boundary conditions. Additionally, more exotic effects such as broken time reversal symmetries due to magnetic ordering could lead to contributions as well[3].

There are many different methods that can be employed to study these various systems, however SHG is a very good tool to use because it is non-invasive, non-destructive and simple[4]; these aspects makes it suitable for more sensitive systems like that of Hg1201. The focus of this paper will be on the experimental technique involved when using SHG, as well as results obtained from studying GaAs (111) and Si (100). Future objectives will be explained at the end of this paper.

2. Optical Second Harmonic Generation and Circular Dichroism
2.1 Second Harmonic Generation

If a bound electron is pictured as a simple harmonic oscillator, then under a weakly intense incident oscillating electric field, the electron will undergo small displacements about its equilibrium position[1]. The electron's response can be described by a linear polarization term:

$$P = \varepsilon_0 \cdot \chi \cdot E$$

Equation 1

However, if the incident electric field intensity is sufficiently large, then the electronic response will be driven into the nonlinear regime, and a more general equation for the electric polarization is required. By taking a Taylor expansion of equation 1, higher order terms can be obtained; in particular, the second order nonlinear polarization term is responsible for SHG. Assuming the incident electric field is sinusoidal, the second order nonlinear polarization takes the form of the following:

$$P_i = \sum_{i=x,y,z} \varepsilon_0 \frac{\chi^{(2)} E_i^{\,2}}{2} (1 - \cos(2 \cdot \omega_i \cdot t + \phi_i))$$

Equation 2

Important to point out is that if the incident electric field is oscillating at a fundamental frequency ω, then the optical response of the system results in an asymmetric charge oscillation about equilibrium. This distribution then reradiates at twice the fundamental frequency, due to the cosine term in equation 2. Figure 1 shows this relationship graphically.
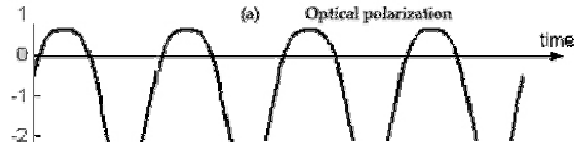
Figure 1: Optical response of charge distribution under a sufficiently intense incident electric field.
(**Reproduced from** http://www.elettra.trieste.it/experiments/beamlines/lilit/htdocs/people/luca/tesihtml/img826.png)

Therefore, materials with a non-zero $\chi^{(2)}$ will allow for SHG. Contributions from these materials to SHG can be due to bulk dipole and quadrupole terms, and/or surface dipole terms resulting from broken inversion symmetry.

However, because the electric field and polarization are vectors and not scalars, they are related through the electric susceptibility tensor, and not just a scalar. Using a tensor is more general because the defined axes of a crystal beget a directional dependence of the nonlinear response of the system.

Circular Dichroism

Before introducing the concept of circular dichroism, a few key terms will be briefly explained for completeness. Setting the input polarization of the laser beam and the output polarization of the SHG response are crucial for distinguishing between surface and bulk terms as well as producing phase shifts between the different contributions of $\chi^{(2)}$.

Three different polarizations are used in order to analyze the system. **P**-polarization is polarization of the electric field parallel to the plane of incidence. **S**-polarization is perpendicular to the plane of incidence. Circular polarization is defined as having perpendicular components of the electric field which are $\pi/2$ radians out of phase with each other; see Fig.2. This phase difference between the two components leads to the resultant electric field vector rotating either clockwise (c.w.) or counter clockwise (c.c.w.). Right-handed circular polarization is the case when the electric field is rotating c.c.w. in the direction of beam propagation ($\mathbf{E_x} + i\mathbf{E_y}$). Left-handed circular polarization is just the opposite ($\mathbf{E_x} - i\mathbf{E_y}$). The difference between these two cases can be thought of as the electric field in the 'y' direction as being π radians out of phase between the two. The following figure displays the relationship between the **s** and **p** components.
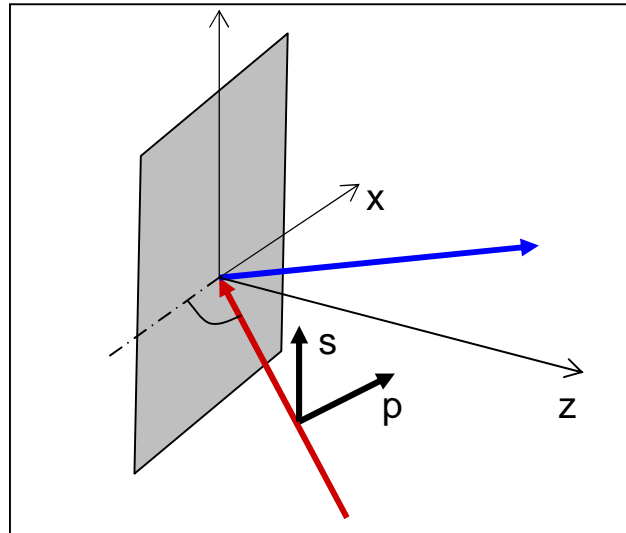
Figure 2: relationship between input laser beam, sample, and SHG response.

Many materials, under appropriate polarization conditions, will generate different SHG intensities between responses induced from left- and right-handed circularly

polarized light. The difference in these intensities divided by their sum is defined as circular dichroism. Under many conditions, circular dichroism can be attributed to phase mismatching between different $\chi^{(2)}$ tensor elements[5].

$$D_c = \frac{I_R - I_L}{I_R + I_L}$$

Equation 3

In equation 3, I_R (I_L) is the intensity generated by right- (left-) handed circularly polarized light.

Because nonlinear effects are usually small, high SHG conversion efficiency is usually obtained by using a long propagation length of the nonlinear medium[6]. Because the incident propagating electric field oscillates at a different frequency than the generated second harmonic field, a phase mismatch with respect to the produced nonlinear waves will be generated. In order for these nonlinear contributions to be significant, the phases of these waves that are generated throughout the entire crystal must all be the same so that the fields add constructively.

This phase matching is obtained by taking advantage of the fact that crystals used for nonlinear properties are birefringent[6]. In a crystal of this sort, with a laser beam incident to the crystal axis at a specific orientation, the refractive indices of the field of fundamental frequency and that of the second harmonic field can become equal, and phase matching will be obtained.

Additionally, phase mismatching also occurs between different tensor elements when the incident electric field is circularly polarized. This is because the different tensor elements are probed with 'x', 'y', or a combination of 'x' and 'y' electric field components (in the beam coordinate system), which are inherently out of phase in this polarization case. This phase mismatching is often the cause of circular dichroism.

3.   Experiment
3.1   Overview of Semiconductors
The two samples that were studied are both semiconductors, yet generate different SHG signals. A semiconductor is a solid whose conductivity is similar to that of an insulator

but can be easily modified to be like that of a conductor. The energy of the electrons levels in an atom is discrete. When forming a solid the density of atoms and electronic energy levels is so large that the electronic states become bands. Each band is separated from the next by band gaps, where the electron is not allowed.
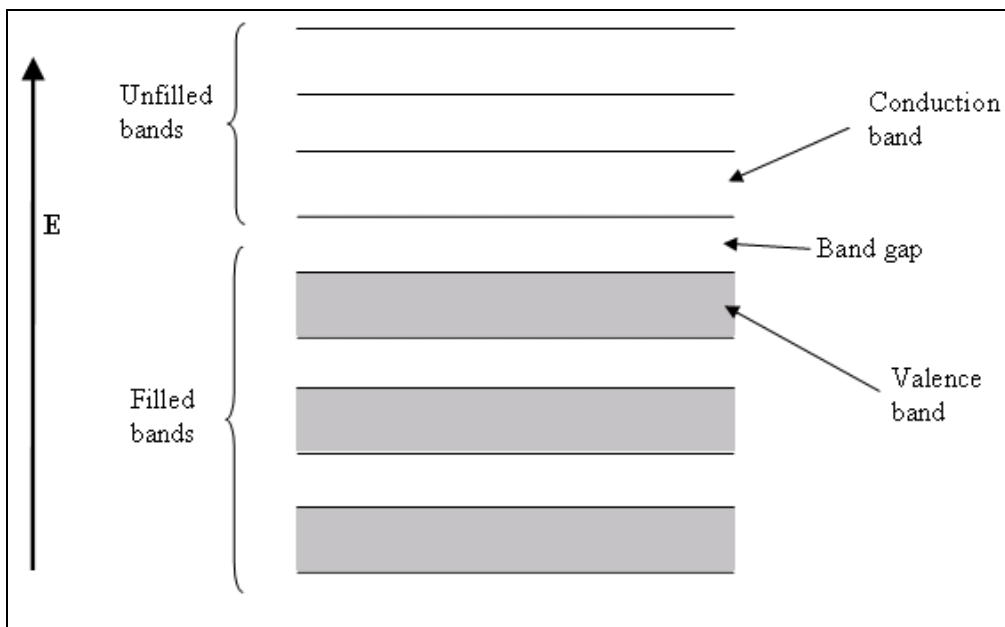
Figure 3: Energy level diagram for a semiconductor. (Reproduced from http://www.chemistrydaily.com/chemistry/upload/a/a3/Semiconductor_band_structure_(lots_of_bands).png)

At low temperature, the energy bands are filled from the ground state up to an energy state within one band, known as the Fermi Energy. All bands below the Fermi energy are valence bands (with bound electrons), and all band above this energy are conduction bands (with free electrons); see Fig.3. For insulators and semiconductors, the Fermi energy lies within a band gap. For these two types of materials to conduct electricity, the electrons need to be provided with a sufficient energy so that they are promoted to the conduction band where they are then able to move. The difference between the two is that semiconductors have much smaller band gaps than insulators. For metals, the Fermi energy level lies within a conduction band, and thus electrons can much more easily move.

During SHG in a semiconductor, two incident photons of similar frequency drive an electronic polarization in the material. The energy of those two photons are converted into a photon at twice the frequency of the incident photons, only as long as the material

allows for a non-zero $\chi^{(2)}$ tensor. The second order nonlinearity is allowed when the crystal's unit cell is non-centrosymmetric. Binary alloy semiconductors such as GaAs have non-centrosymmetric unit cells and elemental semiconductors such as Si exhibit centrosymmetry [6-7].

3.2   Experimental Setup
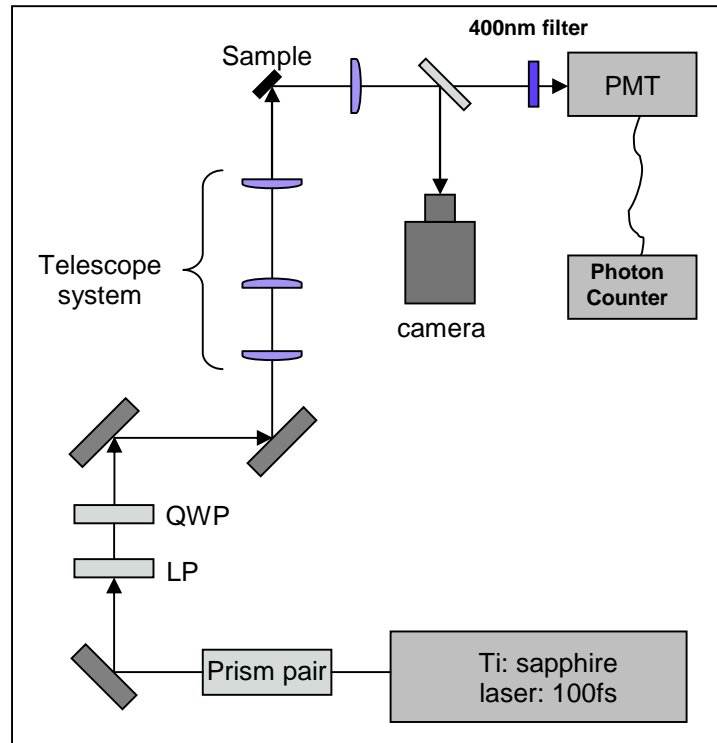
Figure 4: experimental setup

The schematic diagram of the experimental setup is shown in Fig.4. A laser pulse is created using a mode-locked titanium sapphire laser, producing 100 fs pulses at 40 MHz repetition rate, with a central wavelength of 800 nm and a full-width half maximum (FWHM) bandwidth of approximately 11 nm. The average power incident at the sample can be adjusted in a range from 1 – 40 mW. The laser is inherently polarized horizontally with respect to the optical table.

A prism pair, directly after the laser, is used to pre-compensate for positive material dispersion introduced via the various optics. Because the laser pulse is very short in time, its frequency spectrum consists of many different frequency components. Each of these components will travel through materials at different speeds, and thus the

pulse will spread out in time along the optical path. This increased pulsewidth leads to a decreased duty cycle and hence a reduced pulse intensity at the sample. Since the SHG is directly proportional to the square of the electric field (the intensity), this would result in a weaker signal. In order to keep the pulse 100 fs, a prism pair is adjusted to, ideally, exactly cancel the positive dispersion produced by the optics. The pair introduces negative dispersion, and the dispersion is minimized to second order. Using a model from Diels et al.[8], we have calculated that the prism separation must be 297.4 mm and the tip to beam distance through the second prism must be 4.10 mm.

Following the prism pair is a linear polarizer (LP) which ensures that the laser beam is horizontally polarized (or vertical if desired, but a half-wave plate would be needed before the polarizer). The beam then travels through the quarter-wave plate (QWP), which is a birefringent material, such that the electric field of the polarized beam passes 45 degrees between the fast and slow axes of the QWP. Under this condition, the polarized beam can be split into its two components, one along the fast axis, and one along the slow. The phase of one electric field component is then retarded by $\pi/2$, and thus producing circularly polarized light.

The beam then travels through the telescope system to expand the beam before it is focused onto the sample using a graded index lens. Expanding the beam before this final lens makes use of the whole clear aperture and improves focusing. Because the beam profile is Gaussian[9], the focus is not an infinitesimally tight spot, but instead a minimum beam radius, or beam waist.
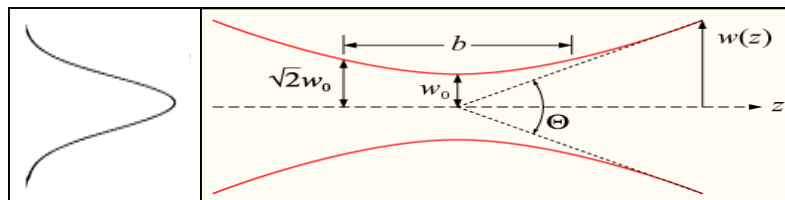
Figure 5: Gaussian beam waist, , relationship to propagation distance. Intensity profile shown on left.

The minimum beam waist is ~10 μm and is positioned directly at surface of the sample so as to be the most intense and resulting in the largest SHG response. The final lens can also be adjusted in all three Cartesian directions to adjust the beam to the center

of the sample (which is important during rotations) and to maximize the focusing (which increases the intensity and therefore SHG response).

The turning mirror directly before the telescope system is mounted on a Newport motorized mount, and allows for scanning of the beam across the sample. This isn't so important when studying the semiconductors because they are spatially isotropic. However, when studying Hg1201, this will be beneficial for finding superconducting domains that will be suitable for analyzing.

The beam is incident on the sample with a polar angle of 45° to the normal, and the generated second harmonic signal is reradiated in the specular direction. The signal is then passed through a 400 nm filter to suppress any remaining 800 nm light and ensure that the photomultiplier tube (PMT) response is strictly due to SHG. The PMT is connected through a discriminator/amplifier box to an HP counter. The discriminator/amplifier box converts the current generated by the PMT into TTL pulses. The discriminator has a variable voltage threshold that can be adjusted to set the lower limit on what is considered a count from the SHG, and what is considered a dark count (counts with no signal). Figure 6 shows data relating the dark counts to the threshold setting. Adjusting the threshold until the counts start to sharply rise minimizes the dark counts while maximizing the signal, resulting in the largest signal/dark count ratio. For this particular PMT setting (-1400V), the discriminator threshold is set anywhere from 1.5 to 2.5. The system was complete covered in a black plastic box to shield the PMT from ambient blue and UV radiation.
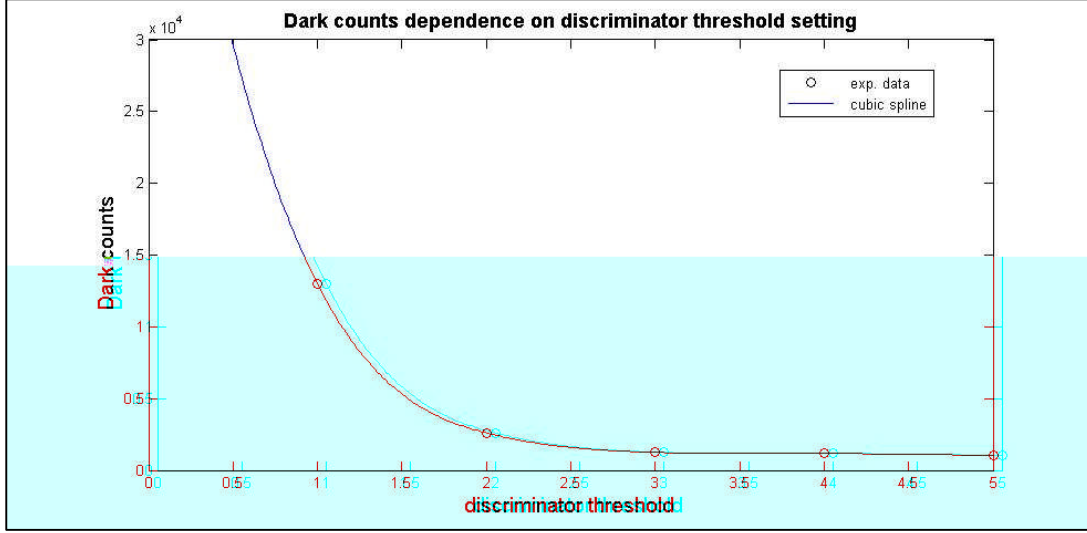
Figure 6: PMT dark counts vs. discriminator threshold setting. PMT is set at -1400V.

4.   Results for GaAs (111)

GaAs (111) is a cubic, non-centrosymmetric crystal, meaning that it has strong bulk dipole contributions to $\chi^{(2)}$. It belongs to the class $\overline{4}3m$, where the $\chi^{(2)}$ tensor looks like the following[6]:

$$
\begin{pmatrix} P_x \\ P_y \\ P_z \end{pmatrix} = \begin{pmatrix} \cdot & \cdot & \cdot & \bullet & \cdot & \cdot \\ \cdot & \cdot & \cdot & \cdot & \bullet & \cdot \\ \cdot & \cdot & \cdot & \cdot & \cdot & \bullet \end{pmatrix} \cdot \begin{pmatrix} E_x^{\ 2} \\ E_y^{\ 2} \\ E_z^{\ 2} \\ E_y E_z \\ E_x E_z \\ E_x E_y \end{pmatrix}
$$

Equation 4

The smaller dots represent zero value, while the 3 larger dots are non-zero and are all equal.

Two polarization conditions were explored for this crystal. First, a **p** input and **s** output polarization where chosen. If the laser beam were incident on the sample normal to the surface, then one would expect the SHG response to exhibit 6-fold symmetry with

respect to the azimuthal angle. However, because the beam is incident at 45° to the surface normal, 6-fold is no longer expected. This is due to the fact that two azimuthal positions 180 degrees apart no longer see the same electric field, as opposed to a beam normal to the surface. Because of this, 3-fold symmetry is expected and measured; see Fig.7. One point to note is that there are still surface dipole contributions to the SHG response; however they are negligible compared to the bulk dipole contribution.
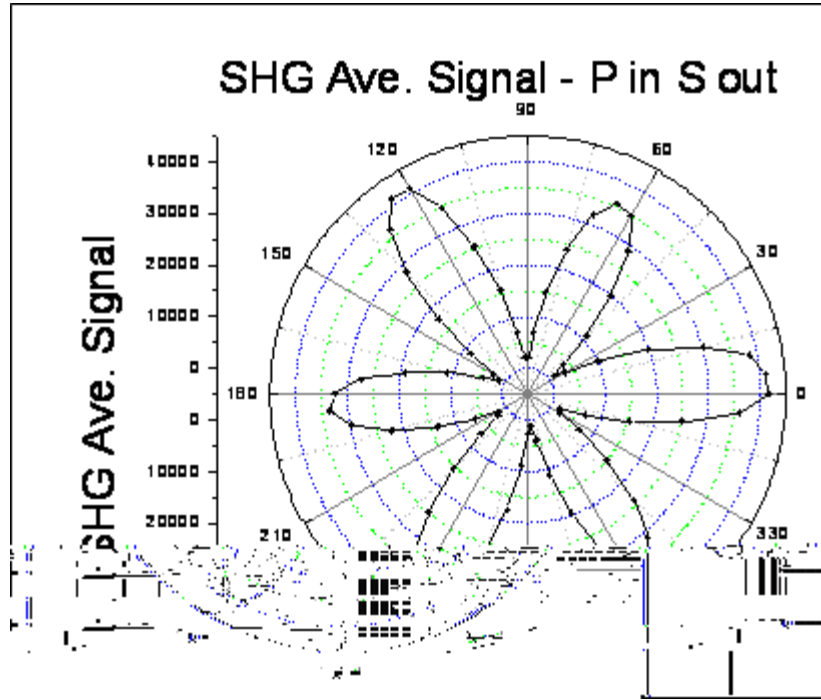
Figure 7: Ave. SHG signal; P polarization in, S polarization out.

However, if the input polarization is now changed from **p** to circular, the relationship between the tensor elements plays a larger role. As mentioned previously, circular polarization results when the $\mathbf{E_y}$ component is $\pi/2$ radians out of phase with the $\mathbf{E_x}$ component. According to equation 4, the 4th and 5th terms in the electric field vector, $\mathbf{E_yE_z}$ and $\mathbf{E_xE_z}$, are out of phase and means the tensor elements will interfere. The interference leads to similar symmetries than the previous polarization conditions.
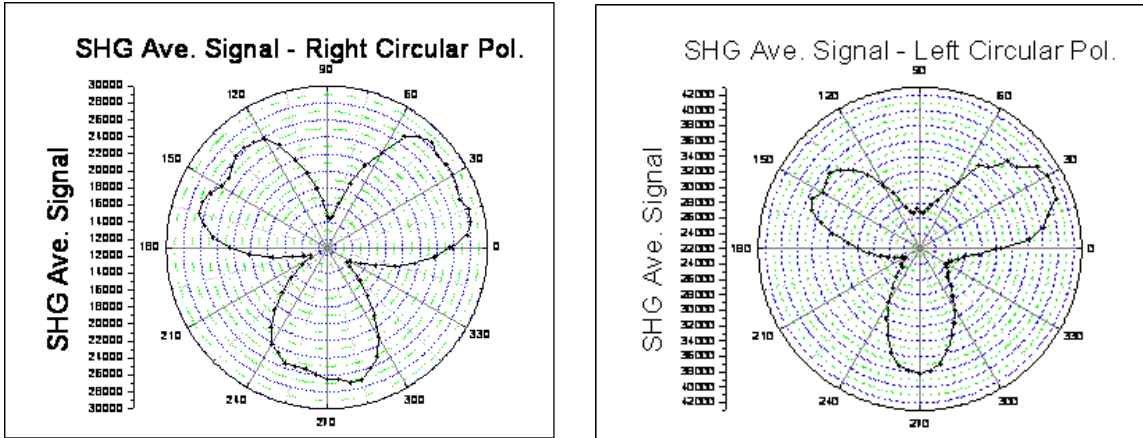
Figure 8: Ave. SHG signal from right- and left-handed circular polarization.

Figure 8 shows the average signals obtained under right- and left-handed circular polarization of the incident electric field as a function of sample azimuthal angle. It may not be evident, but the intensity of the SHG response is different between the right- and left-handed circular polarizations – the left-handed signal is significantly larger. This difference in intensities leads to circular dichroism, explained earlier.
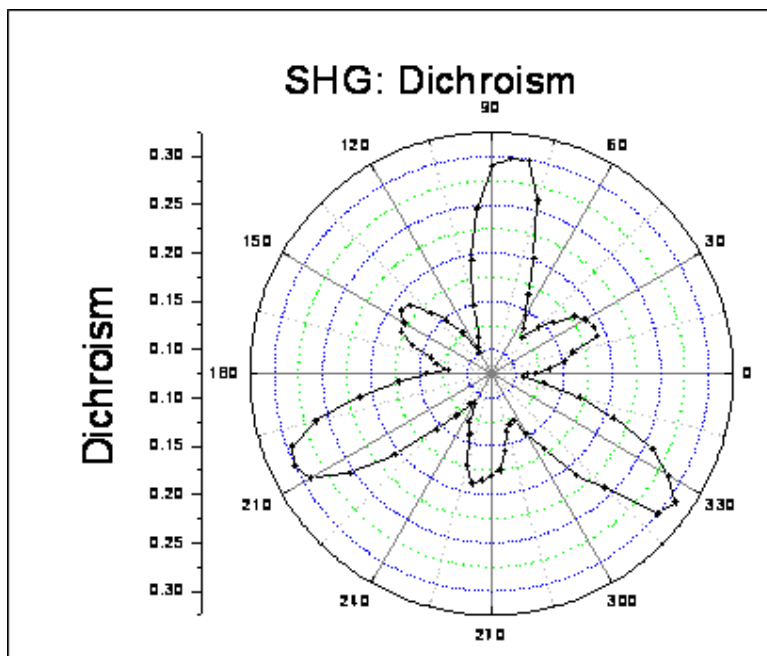
Figure 9: Circular dichroism for GaAs (111). Output polarization is S.

Figure 9 shows the resultant circular dichroism as a function of sample azimuthal angle, under circular input and **s** output polarization conditions. With **p** input and **s** output polarizations, the tensor elements exhibited 3-fold symmetry as well. However, with circular input polarization instead of **p**, the figures for the average SHG response exhibit only 1 set of 3-fold symmetric lobes. However, the figure for dichroism shows two sets of 3-fold symmetric lobes.

5.   Results for Si (100)

Si (100) is a cubic, centrosymmetric crystal[7], meaning a bulk dipole exhibits inversion symmetry, and thus cannot contribute to $\chi^{(2)}$. However, very weak bulk quadrupole terms and strong surface dipole terms from broken inversion symmetry can contribute to the second order nonlinear tensor, and thus Si (100) will produce SHG and also exhibit circular dichroism.

$$
\begin{pmatrix} P_x \\ P_y \\ P_z \end{pmatrix} = \begin{pmatrix} \cdot & \cdot & \cdot & \cdot & \bullet & \cdot \\ \cdot & \cdot & \cdot & \bullet & \cdot & \cdot \\ * & * & \circ & \cdot & \cdot & \cdot \end{pmatrix} \cdot \begin{pmatrix} E_x^{\,2} \\ E_y^{\,2} \\ E_z^{\,2} \\ E_y E_z \\ E_x E_z \\ E_x E_y \end{pmatrix}
\qquad \textbf{Equation 5}
$$

Referring to equation 5, setting the output polarization to **s**, only the $\chi^{(2)}_{15}$ and $\chi^{(2)}_{24}$ terms are non-zero. As before, only the 4th and 5th electric field vector terms contribute to SHG, allowing both the E_yE_z and E_xE_z terms to contribute to the second order polarization. Two different conditions were studied – **p** input polarization and circular input polarization.

Because the input polarization is circular, the 'x' and 'y' components of the electric field are out of phase, leading to interference between the two non-zero tensor elements. Theory developed by *Sipe et al.*[10] claim that under these conditions, both bulk quadrupole and surface dipole terms are non-zero, and the interference between these

terms leads to a (sin(4φ)+const.) relationship, where φ is the azimuthal angle. Since the intensity of the SHG response is measured, squaring this function results in a 4-fold symmetry.
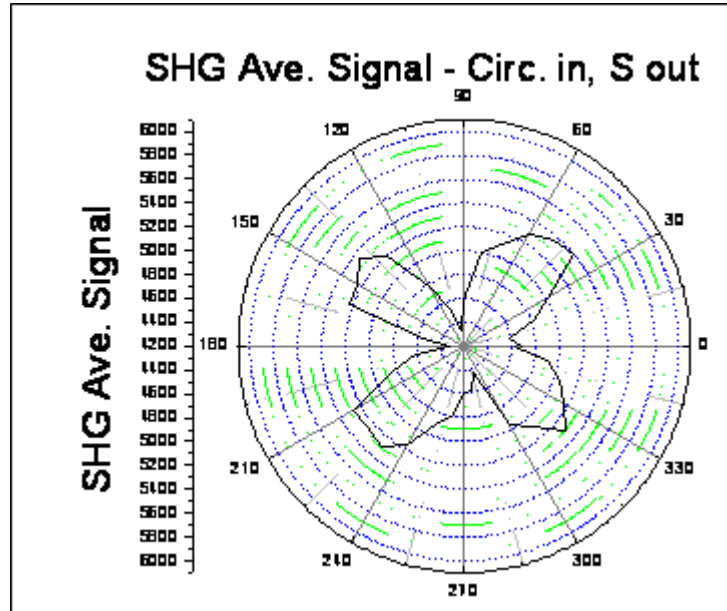
Figure 10: Ave. SHG signal; Circular Polarization in, S polarization out.

Figure 10 shows the average SHG signal for circular polarization input and **s** polarization output as a function of sample azimuthal angle. The plot looks slightly irregular, which is more than likely due to not using enough azimuthal data points, as well as using too low of a counting time and counting sessions per azimuthal position. The use of few points was done due to time constraints; however for the purpose of obtaining symmetry information, the above plot suffices.

If the input polarization is set to **p**, then the surface dipole contribution is suppressed and the bulk quadrupole contribution is isolated. *Sipe et al.* determined theoretically that the intensity under this condition should behave like $\sin^2(4\varphi)$, which is an 8-fold symmetric function. However, through experience, this 8-fold relationship cannot be obtained if even the slightest amount of **p** output polarization leaks through the polarizer to the PMT. Because the bulk quadrupole contribution is so weak and the surface dipole is comparatively large, any bit of **p** polarization at the output will result once again in the 4-fold symmetry obtained when both terms are present. The output polarizer had to be adjusted within tenths of a degree in order to obtain the 8-fold symmetry, shown in Fig.11.
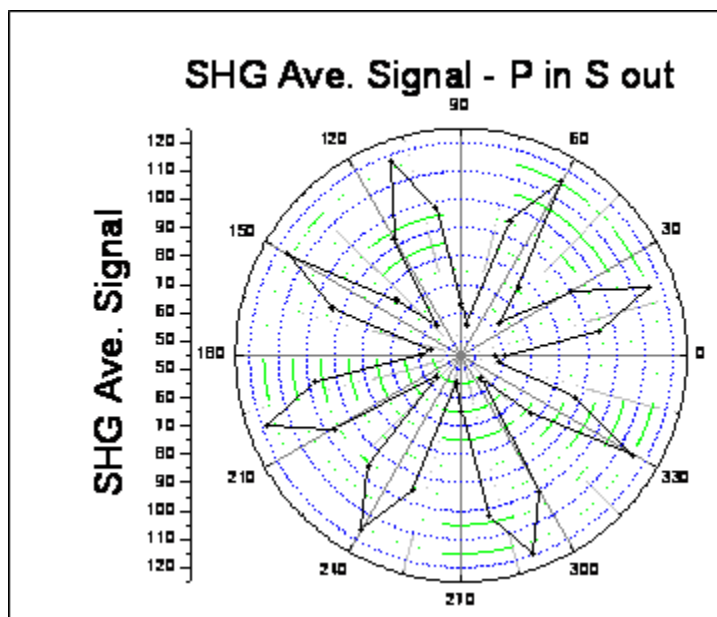
Figure 11: Ave. SHG signal; P input polarization, S output polarization.

Again, one will notice that the lobes look sharp, and this is due to not using a sufficient amount of azimuthal data points. Nonetheless, the 8-fold symmetry can be seen, consistent with the theory.

It is important to note that the errors associated with each data point, on average, are anywhere from 5-15% of the SHG signal itself (1 standard deviation) for the Si (100) measurements. These can be greatly reduced by using longer photon counting times and more counting sessions per azimuthal data point. Counting more and longer is extremely important for samples that exhibit a very weak SHG response, like that of Si (100).

Additionally, under conditions of **p** input polarization and **s** output polarization, both the bulk and surface terms are present. Phase-mismatched interference between these two contributions results in a difference in SHG intensities for right- and left-handed circular polarization – leading to circular dichroism; see Fig.12. Notice the 4-fold symmetry.
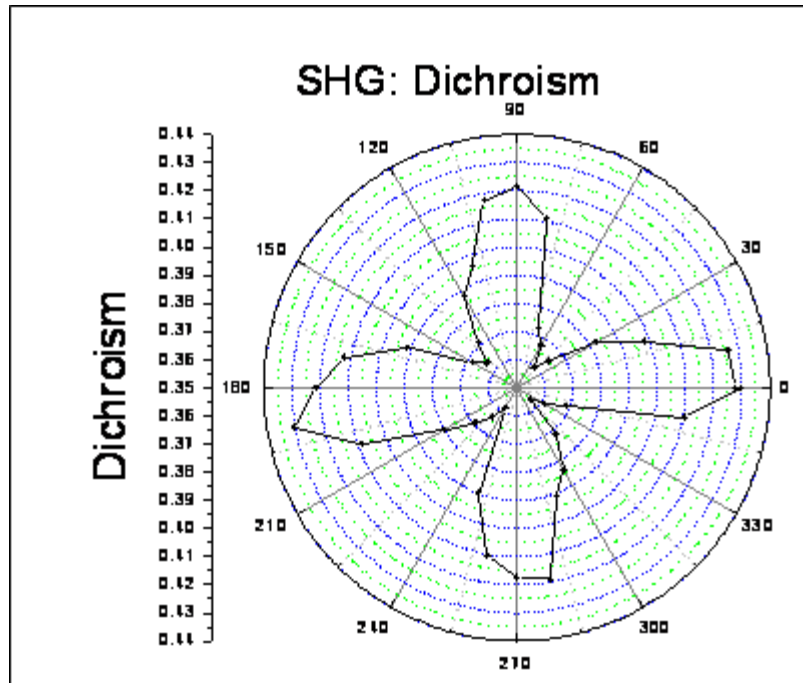
Figure 12: Circular Dichroism for Si (100).

6.   Conclusions and Future Work

The relationship between second order nonlinear tensor elements and bulk and surface contributions of GaAs (111) and Si (100) have been explored. Because GaAs (111) is a non-centrosymmetric crystal, bulk electric dipole contributions are strong and overshadow surface dipole contributions. The SHG response exhibits 3-fold symmetry for circular/**p** input and **s** output polarizations as a function of azimuthal angle; additionally, circular dichroism was observed. Si (100) is a centrosymmetric crystal, and thus displays very strong surface dipole contributions to the second order nonlinearity, due to broken inversion symmetry.   The surface terms exhibit 4-fold symmetry. However, under **p** input and **s** output polarizations, weak bulk quadrupole contributions become evident and exhibit 8-fold symmetry.

Studying the aforementioned systems has allowed for the characterization and optimization of an experimental setup that is capable of exploring more complicated systems. The setup is equipped to measure the SHG response as a function of azimuthal angle as well as temperature. Also, because of the inclusion of the telescope system, the

input laser beam can be raster scanned across samples, which will be very useful when studying superconductors.

We are beginning to study the low temperature dependence of the SHG response of Si (100). To the best of our knowledge, no studies have been performed on this and results could prove to be interesting. Additionally, this experiment will allow for the setup to be tested at low temperatures and optimized for samples that exhibit a low SHG response.

The systems focused on in this paper are fairly simple and well understood. A more exciting system to study would be one not only where crystal symmetries and surface boundary conditions contribute to nonlinear processes, but where electron correlated events contribute as well; Hg1201, a high T_c superconductor, will soon be studied. A search for possible magnetic ordering and broken time reversal and inversion symmetries will be performed. Data from this experiment can possibly prove or refute different theories about the underlying properties that are the origin for such a high critical temperature.

References:

[1]   M. Fox, *Optical Properties of Solids* (Oxford, 2001).

[2]   Zhao et al., Adv. Mater. **18**, 3243-3247 (2006).

[3]   M. E. Simon, C. M. Varma, Phys. Rev. B **67**, 054511 (2003).

[4]   Y.R. Shen, *Principles of Nonlinear Optics* (Wiley, 1984).

[5]   G. J. Simpson, J. Chem. Phys. **117**, 3398 (2002).

[6]   A. Yariv, *Quantum Electronics* (Wiley 1989).

[7]   Li et al., Phys. Rev. Lett. **89**, 022102 (2006).

[8]   J. C. Diels and W. Rudolph, *Ultrashort Laser Pulse Phenomena* (Academic, 1996).

[9]   W. T. Silfvast, *Laser Fundamentals*, (Cambridge, 1996).

[10]   J. E. Sipe et al., Phys. Rev. B **35**, 1129 (1987).